Riddles of the sphinx tilings

Greg Huber*
Chan Zuckerberg Biohub – San Francisco, 499 Illinois Street, San Francisco, CA 94158, USA

Craig Knecht†
691 Harris Lane, Gallatin, TN 37066, USA

Walter Trump‡
Department of Physics, Gymnasium Stein, Faber-Castell-Allee 10, 90547 Stein, Germany

Robert M. Ziff§
Center for the Study of Complex Systems and Department of Chemical Engineering, University of Michigan, Ann Arbor, MI 48109-2800, USA

(Dated: May 2, 2023)

The sphinx tile, a hexiamond composed of six equilateral triangles in the shape of a sphinx, has interesting and complex tiling behavior due to its chirality and asymmetry. Sphinx-shaped regions ("sphinx frames") can be tiled in quasicrystalline "rep-tiles" when the order is 2^n, but also in more complex and disordered tilings within sphinx boundaries of all orders. For frames up to order 13 we carry out exact enumeration using *accelerated backtracking*, *seam*, and *dangler* algorithms to find the number of tilings, while for larger frames we introduce a Monte Carlo (MC) method to create randomized tilings. Key to the latter is the identification of fundamental shapes (*polyads*) that have multiple tilings and allow a rejection-free MC move once the polyad is identified. We also introduce an Ising-like chiral interaction energy between neighboring sphinx tiles and study how the system behaves as a function of temperature; at low temperatures, chiral ordering is found.

Introduction. The study of tilings has been a fundamental and fertile part of statistical mechanics since at least 1937 with the introduction of the dimer tiling [1], which was solved exactly for the square lattice in 1961 [2, 3]. Dimer tilings are related to Pfaffian solutions of the Ising model [4] and have reappeared in many guises [5–9]. When the region tiled is the shape of an Aztec diamond, vast simplifications in the enumeration occur, phase ordering emerges, and the beautiful Arctic Circle theorem obtains [10–13].

Interest in more complex tiles formed of connected polygons was reignited by Golomb [14, 15], who introduced "polyominoes" as generalizations of dominoes. Polyominoes are composed of two or more squares connected together—the shapes in the game *Tetris* are examples of tetrominoes. In statistical mechanics, polyominoes are known as "lattice animals" and have been studied extensively in relation to percolation, the Ising model, and other problems. Tiles made of equilateral triangles are called "polyiamonds" as a generalization of diamonds [16]. When the number of triangles is six, the shapes are called *hexiamonds*, and there are twelve distinct configurations, all of which have been assigned names [16, 17]. Here we consider just one of those hexiamonds, the sphinx tile, illustrated in Fig. 1. The sphinx has the interesting property that it has no symmetry and has an inherent chirality. When it is placed on a triangular lattice, there are twelve possible embeddings (states) of a sphinx, six of each chirality, which we call left ("L") and right ("R"), depending on the location of the head of the sphinx when oriented horizontally (Fig. 1.) The shape of the sphinx leads to frustration as seen in problems of packings and glasses.

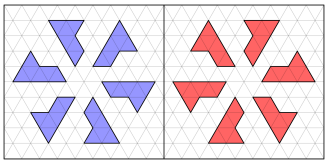

FIG. 1. L-sphinxes (left) and R-sphinxes (right), showing the six orientations of each.

In the past, the sphinx has garnered interest because it is a so-called "rep-tile" (following Golomb) that can be tiled by four smaller sphinxes, as in the order-2 tiling in Fig. 2 [18]. This allows one to recursively create large tilings with a self-similar or quasicrystalline form [19–22]. Quasicrystals have occurred in many contexts [23–25], including the recent discovery of a planar tiling that uses a single tile and its mirror image [26].

Here we are interested in enumerations of sphinx tilings given a boundary (frame) which the sphinxes must fill without leaving any spaces. We consider only boundary frames being in the shape of a sphinx. In rep-tiles, the number of possible tilings is just one, but for general tilings of a sphinx frame, the number of tilings grows rapidly with the order. Here order represents the num-

* gerghuber@gmail.com
† craigknecht03@gmail.com
‡ w@trump.de
§ rziff@umich.edu

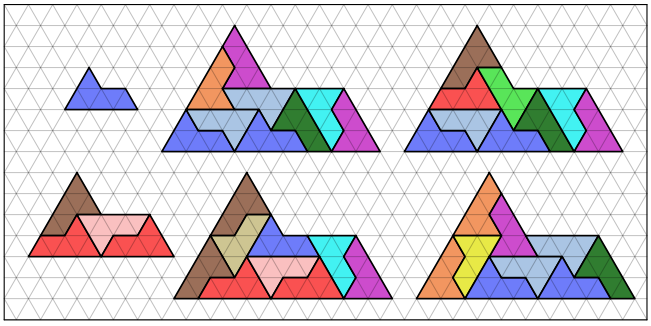

FIG. 2. All sphinx tilings of order 1, 2 and 3. Here the 12 colors represent the 12 possible tile orientations as shown in Fig. S2 in the Supplemental Material (SM).

ber of triangle edges on the tail end of the sphinx, and can have values 1, 2, 3, ... In fact, a frame in the shape of a sphinx of any order can be tiled by elementary sphinxes, a result that can be proven by a simple inductive argument. Such is not the case for many other frame shapes, where only certain orders can be tiled by sphinxes, like triangles (12, 24, 36, ...) and regular hexagons (6, 8, 10, ...). Previously, sphinx tiles in sphinx frames have been enumerated up to order 8 [27]. Here we extend that to order 13.

Algorithms. For the enumerations of tilings of sphinx frames up to order 7, we used a "backtracking" method, where we proceed across the triangles of the frame in a row-by-row manner and recursively go back to find other tilings. This algorithm generates every possible complete tiling, and as a consequence it is limited in terms of the order it can handle. To increase the speed of the algorithm and reduce memory, we describe both the frame and tiles by 64-bit binary integers, where each bit represents the state of an underlying grid triangle.

For higher-order frames, we have developed techniques to enumerate tilings without explicitly generating each of them. First we describe our "seam method." While the sphinx frame itself has no symmetry, it does have a decomposition into two symmetrical hemisphinxes (trapezoids), identical except for their orientation and connecting edge. A seam starts at the sphinx-neck point and meanders along sphinx-tile boundaries until it partitions the base in the ratio 1:2, as shown in Fig. 3. To simplify the enumeration, we only let the seam meander within a single hemisphinx; we choose the right-hand hemisphinx when the frame is oriented in the "canonical" state, as in Fig. 3. In principle, the number of seams increases very rapidly with the size of the sphinx; however, most seams do not admit a tiling on both halves. Those that do admit a tiling are extremely rare and can be enumerated individually. For order 8, for instance, the number of "legal" seams is 1468 out of 8619612 possible meanders. For each possible partition, we determine the number of tilings of the two areas and multiply the two together, and add all products to get the total number of tilings for that seam. Finally, we sum over all possible seams. In principle, this method allows one to generate all tilings by convolution of the tilings from each side of the seams.

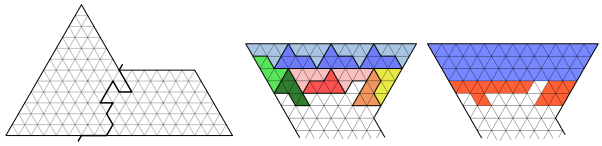

FIG. 3. Left: Illustration of the seam method, where the seam is shown in heavy black. Enumerations of the two regions on either side of the seam are shown in SM. Middle and right: A complete tiling of the first 3 rows using the dangler method, and the associated dangler shape (red sphinxes).

For $n > 11$, further improvements are necessary because of memory constraints in the above two methods. Here we start with the top row as shown in Fig. 3. After covering all triangles of a certain row r, we consider all possible shapes built by the covered triangles of the next two rows, but only accept those shapes that allow further tiling of row $r + 1$. We describe each of these "dangler" shapes by a binary representation, with one integer for each of the two rows. Unlike with a standard backtracking method, we do not have to continue for each tiling. We save a large amount of computing time, because in most cases the number of danglers is much smaller than the number of tilings.

With the dangler method, it takes less than a second to calculate the number of sphinx tilings of an 8-sphinx, and all results from our previous methods up to order 11 could be confirmed. Order 12 takes about 3 hours and order 13 about 3 days using up to 6 cores on a desktop computer. The bottleneck of the calculation is the necessary amount of memory for saving the danglers, which in practice limits this method to order 13. The dangler method is much faster than the seam method, but it does not explicitly produce all tilings, and is mainly useful for enumeration. The seam method can be split into several independent parts (corresponding to the different seams), and has the advantage that tilings can be saved and used for further study.

Results. The final enumeration results for the number of tilings N_n from all three methods are listed in Table I and have been posted on [28]. For $n = 13$, the number of tilings is greater than 10^{30}, highlighting the power of our methods. The asymptotic behavior of N_n can be exhibited by plotting its logarithm as a function of n^2, the number of sphinx tiles in an n-sphinx. This is shown in Fig. 4. A straight line on this plot is the expected behavior based upon the dimer tiling solution [2, 3, 29] and a lower bound [30], and that behavior is confirmed. The data points (red circles) appear to show a periodicity of 3, such that sphinx frames of order $3k$ have more tilings than expected when looking at the two previous orders; we have no definitive explanation for this intriguing behavior. The slopes of these lines approach 0.425(2), implying an effective entropy that grows, to leading order,

TABLE I. Number of tilings of a sphinx frame of order n.

n	tilings
1	1
2	1
3	4
4	16
5	153
6	71 838
7	5 965 398
8	2 614 508 085
9	9 822 629 511 079
10	28 751 930 151 895 611
11	162 231 215 752 303 027 270
12	32 813 942 272 624 544 838 651 213
13	1 257 159 787 425 487 037 702 548 758 466

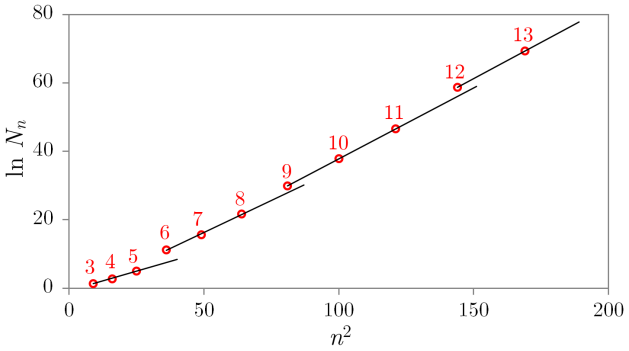

FIG. 4. The log of the number of tilings N_n as function of the square of the order n (n is shown in red).

as $S = k_B \ln N_n$ with $N_n = \exp(0.425\, n^2) = \sigma^{n^2}$ where $\sigma = 1.53(1)$ and n^2 is the area (see SM). Here we are assuming that all configurations are equally likely (equal energy), in which case the partition function is equal to the total number of tilings.

In Fig. 5, we show the density of occurrence of the 36 suitable sphinx states (including each part of the sphinx) on each triangle in the order-7 frame.

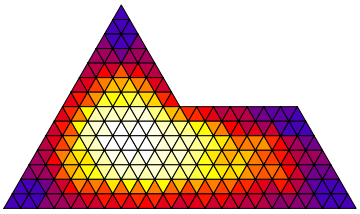

FIG. 5. The order-7 sphinx. Colors represent for each triangle the number of the 36 different ways in which it is covered by sphinx tiles as shown in Fig. S5, when the set of all order-7 tilings is considered, where white represents the maximum (36) and indigo represents the minimum occurrence (4).

We note that once low-order tilings have been identified, it is possible to carry out a general inflation or substitution process to generate higher-order sphinx tilings, as a generalization of the rep-tile process. For example, each of the 4 tilings of the 3-sphinx can be tiled with any of the 16 tilings of order 4, yielding 262144 tilings of the 12-sphinx. These are, of course, an insignificant fraction of the $3.28 \cdot 10^{25}$ tilings of the 12-sphinx.

Types of sphinxes. We define a sphinx of left chirality ("L") as one in which the "head" of the sphinx is on the left-hand side, when the base of the sphinx is horizontal and the sphinx is upright, and likewise for a right ("R") chirality sphinx; see Fig. 1. This designation is independent of the embedding on a lattice. We also define "A" ("up") and "V" ("down") triangles, and A and V sphinxes based on the direction of the head.

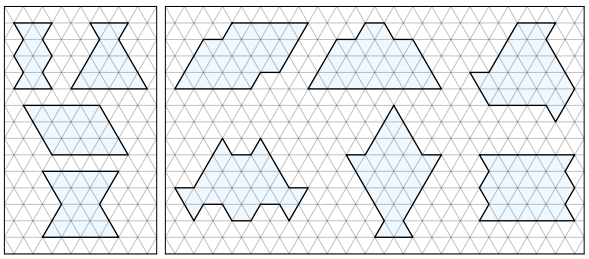

FIG. 6. Fundamental polyads of size 2, 3, 4, 4 (on left) and size 6 (on right).

Polyads. We define a *polyad* of size n as a simply connected polyiamond that consists of $6n$ triangular cells and can be tiled by n sphinx tiles. The polyad is the frame of the polyiamond, and does not refer to any specific tiling. Two polyads are considered *equal* if they can be transformed into each other by rotation, reflection or translation. Due to rotation or reflection, a polyad can have up to 12 different states. Two tilings of a given polyad are *disjoint* if there are no sphinx tiles in the same position and orientation in the two tilings. Two *sets of tilings* of the same polyad are disjoint if each tiling of the first set is disjoint to each tiling of the second set. A *fundamental polyad* has more than one tiling that can be split into two disjoint sets of tilings. (Figs. 6, 7). Within each set there may be tilings that are not disjoint from each other (Fig. 8). On the other hand, both sets may be split in further disjoint sets. However, we have found only one fundamental polyad, the "mystical triode," with more than two mutually disjoint sets of tilings (Fig. 9).

A mirror reflection of a tiling of a symmetric frame can produce a distinct tiling (see axially symmetric examples in Figs. 6), and such polyads can be fundamental. The smallest size where asymmetric fundamental polyads occur is 7 (Fig. 8). As we shall see below, fundamental polyads will play a central role in our method to switch from one tiling to another without re-tiling the whole frame of the system.

All fundamental polyads up to size 6 were found exhaustively and their statistics are listed in table II. The spectra of polyads in tilings of sphinx frames of order 5, 6 and partial results for order 7, are shown in Fig. 10.

TABLE II. Polyads (frames) of size $n = 1$ to 6 and their properties. We also show in the third column the total number of polyiamonds [31], with the last value an estimate based upon extrapolation.

n	Name	Polyiamonds with $6n$ cells and no holes	Polyads	Polyad tilings	Polyads with more than one tiling	Fundamental polyads	Fund. polyad tilings
1	Monad	12	1	1	0	0	0
2	Dyad	3 226	46	47	1	1	2
3	Triad	1 484 738	1 868	1 893	25	1	2
4	Tetrad	753 060 469	98 733	100 687	1 940	2	4
5	Pentad	401 510 058 179	5 449 410	5 589 771	138 865	0	0
6	Hexad	$\approx 2.3 \cdot 10^{14}$	311 784 564	321 765 736	9 816 368	6	14

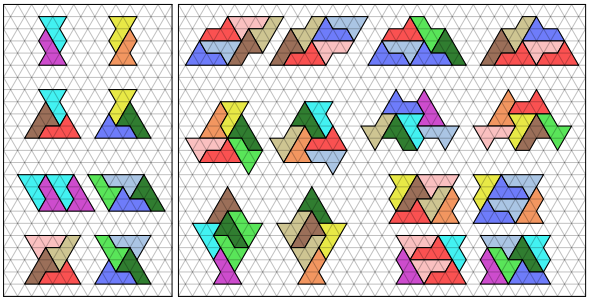

FIG. 7. Tilings of the 4 fundamental polyads of size 2, 3, 4, 4 (left) and the 14 tilings of the 6 fundamental hexads (right)

There are ten fundamental polyads of size 1 to 6, as shown in Fig. 6. Each of these can be tiled in more than one distinct way. We call the fundamental dyad (size 2) "bowtie," the fundamental triad (size 3) "erlenmeyer," and the two fundamental tetrads (size 4) "3×4 parallelogram" and "hourglass." Fundamental monads and pentads do not exist. Polyads of higher order are given in the SM.

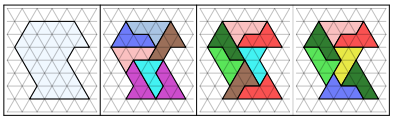

FIG. 8. A non-symmetric fundamental heptad (polyad of size 7) with 3 tilings. The first one is disjoint to the others (meaning that no two tiles are in the same position), but tilings 2 and 3 are not disjoint to each other.

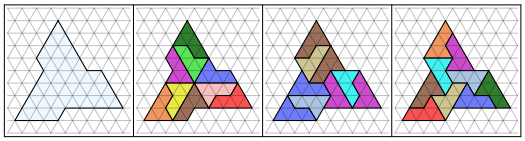

FIG. 9. The "mystical triode," a 3-fold symmetric fundamental ennead (polyad of size 9) with 3 mutually disjoint tilings.

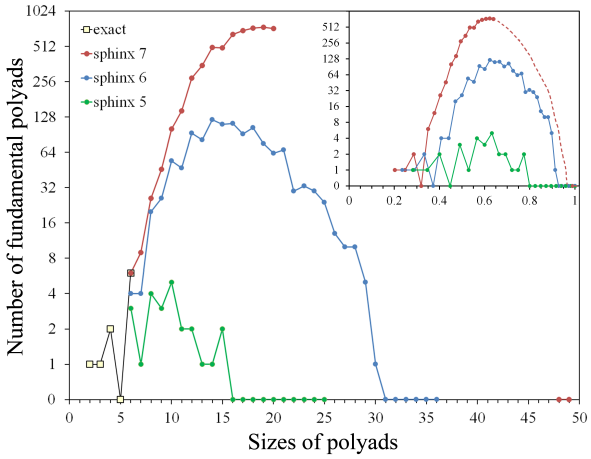

FIG. 10. Spectrum of fundamental polyads found in the tilings of sphinx frames of orders 5, 6 and 7. Inset shows a scaling plot of the number vs. $\sqrt{\text{size}}/\text{order}$, with a dashed line connecting the measured data for size ≤ 21 to the two points at size 48 and 49. The vertical scale is logarithmic except for the point 0 which is included.

Monte Carlo method. Using the concept of fundamental polyads, we developed a Monte Carlo method to generate other tilings from a given tiling. In the simulation, we pick one of the polyads randomly (weighting the larger polyads with lower probability) and search for the occurrence of that particular polyad. If none is found, we try a different polyad; otherwise, if more than one is found, we pick one randomly and replace it with another tiling of that fundamental polyad. A larger frame will typically include many fundamental polyads, and by going through this process we can generate a large number of different tilings. A typical tiling of a 23-sphinx is shown in Fig. 11. For sphinx frames of order up to 6, we can be guaranteed that all possible tilings can be generated by the MC method, because in those cases we know all the tilings, and we can create small sets of fundamental polyads that are sufficient to generate all the rest starting from a single tiling. (We know all the fundamental polyads of size 6, but not all of size 7.) We just need a small subset—polyads up to size 11—to find all tilings for frames of order up to six. For larger frames, it is an open question whether a limited set of fundamental polyads is

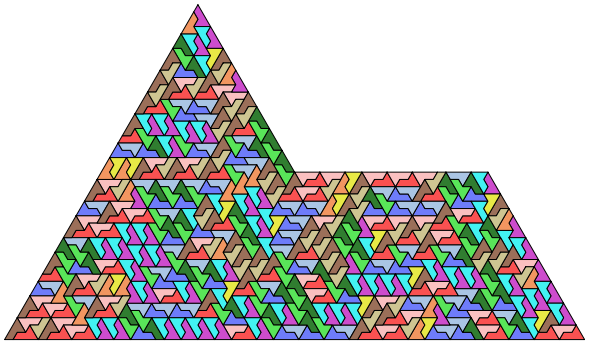

FIG. 11. A typical MC tiling of a 23-sphinx.

sufficient to find all the tilings.

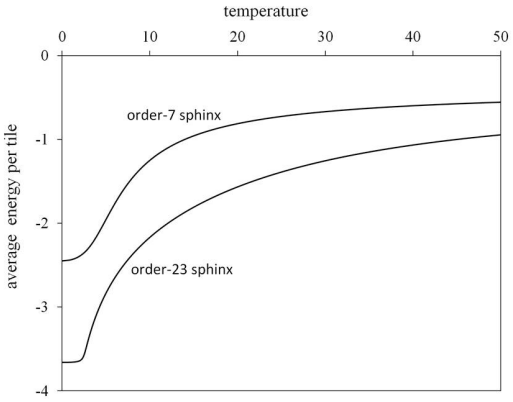

FIG. 12. Energy per tile vs. k_BT/J of tilings of a 23-sphinx based on 10^9 MC samples, and the exact enumeration of the 7-sphinx.

Energetics. Finally, we can include an interaction energy in our system to study the effects of temperature on the equilibrium chirality behavior of the tilings. To define this energy, we consider the chirality of the sphinx, and assign an energy $-J$ to each edge of length 1 between two touching sphinxes if the chiralities are the same, and $+J$ if the chiralities are different. Then, for $J > 0$, we expect that at lower temperatures the system will condense into a phase of a single chirality. Now we carry out the same polyad-based MC simulation as above, but add the Metropolis acceptance criterion based upon the changes of the energy associated with a given trial move [32]. This system is similar ice-type lattice models where the state of a neighboring site is restricted by the state of a central reference site [33, 34]. One difference in the sphinx case is that not all neighboring sphinxes impinge on a given sphinx in equal measure—neighboring sphinxes can share one, two or three common edges. Another difference is that we have a much richer variety of neighbor configurations than in ice-type models.

The resulting average energy is shown in Fig. 12. To find this curve, we carried out our MC algorithm at high temperatures, so that all states were equally likely, and sampled the distribution $n(E)$ of the number of states at energy E, which we used to calculate $E(T)$. For low E we extrapolated the behavior to our estimated minimum energy of $-1850J$, while the lowest energy we found in the MC was $-894J$. Exact results for sphinx or order 7, including the net chirality, are shown in the SM. Further study of this behavior is left for the future.

In conclusion, the tilings of sphinxes form a rich set of problems with connections to statistical physics and mathematics. We developed a Monte Carlo method, based upon the fundamental polyads, that allows random tilings to be generated and the thermodynamic behavior of a system with energetics to be studied. Several models of physical systems, such as capsids [35, 36], are examples of practical applications of such investigations.

Acknowledgments. We thank Artem Ripatti (Ufa State Aviation Technical University, Russia) for independently confirming our results of the sphinx tilings up to order 12, Toshiki Saitoh (Kyushu Institute of Technology, Japan) for helpful correspondence, and Douglas Hofstadter (Indiana Univ.) for a careful reading of our paper.

[1] R. H. Fowler and G. S. Rushbrooke, An attempt to extend the statistical theory of perfect solutions, Trans. Faraday Soc. **33**, 1272 (1937).
[2] H. N. V. Temperley and M. E. Fisher, Dimer problem in statistical mechanics—an exact result, Phil. Mag. **6**, 1061 (1961).
[3] P. Kasteleyn, The statistics of dimers on a lattice: I. The number of dimer arrangements on a quadratic lattice, Physica **27**, 1209 (1961).
[4] M. Kac and J. C. Ward, A combinatorial solution of the two-dimensional Ising model, Phys. Rev. **88**, 1332 (1952).
[5] E. H. Lieb, Solution of the dimer problem by the transfer matrix method, J. Math. Phys. **8**, 2339 (1967).
[6] V. B. Priezzhev and P. Ruelle, Boundary monomers in the dimer model, Phys. Rev. E **77**, 061126 (2008).
[7] M. Loebl, 2d Ising and dimer models, in *Discrete Mathematics in Statistical Physics: Introductory Lectures* (Vieweg+Teubner, Wiesbaden, 2010) pp. 157–171.
[8] A. M. Pham, A Pfaffian formula for the Ising partition function of surface graphs, J. Stat. Mech.: Th. Exp. **2020**, 083103 (2020).
[9] D. Dhar, Self-organized critical state of sandpile automaton models, Phys. Rev. Lett. **64**, 1613 (1990).
[10] W. Jockusch, J. Propp, and P. Shor, Random domino tilings and the arctic circle theorem, preprint arXiv: **math/9801068** (1995).
[11] N. Elkies, G. Kuperberg, M. Larsen, and J. Propp, Alternating-sign matrices and domino tilings. I, J. Algebraic Combinatorics **1**, 111–132 (2023).
[12] P. L. Ferrari and H. Spohn, Domino tilings and the six-

vertex model at its free-fermion point, J. Phys. A: Math. Gen. **39**, 10297 (2006).
[13] R. W. Kenyon and D. B. Wilson, Boundary partitions in trees and dimers, Trans. Amer. Math. Soc. **363**, 1325 (2011).
[14] S. W. Golomb, Checker boards and polyominoes, American Math. Monthly **61**, 675 (1954).
[15] S. W. Golomb, *Polyominoes: Puzzles, Patterns, Problems, and Packings* (Princeton Univesity Press, Princeton, NJ, 1994).
[16] T. H. O'Beirne, Puzzles and paradoxes 44: Pentominoes and hexiamonds, New Scientist **12**, 316–317 (1961).
[17] E. Weisstein, "Hexiamond" from Wolfram Mathworld, mathworld.wolfram.com/Hexiamond (2023).
[18] M. Gardner, *Riddles of the Sphinx, and Other Mathematical Puzzle Tales* (Mathematical Association of America, 1987).
[19] C. Godreche, The sphinx: a limit-periodic tiling of the plane, J. Phys. A: Math. Gen. **22**, L1163 (1989).
[20] J.-Y. Lee and R. V. Moody, Lattice substitution systems and model sets, Discrete & Computational Geometry **25**, 173 (2001).
[21] C. Goodman-Strauss, Matching rules for the sphinx tiling substitution, preprint arXiv: **1608.07168** (2016).
[22] C. Goodman-Strauss, Lots of aperiodic sets of tiles, J. Combinatorial Theory, Series A **160**, 409 (2018).
[23] R. Penrose, Pentaplexity, a class of non-periodic tilings of the plane, Math. Intelligencer **2**, 32 (1979).
[24] A. Haji-Akbari, M. Engel, A. S. Keys, X. Zheng, R. G. Petschek, P. Palffy-Muhoray, and S. C. Glotzer, Disordered, quasicrystalline and crystalline phases of densely packed tetrahedra, Nature **462**, 773–777 (2009).
[25] M. Senechal, *Quasicrystals and Geometry* (Cambridge University Press, 1995).
[26] D. Smith, J. S. Myers, C. S. Kaplan, and C. Goodman-Strauss, An aperiodic monotile, preprint arxiv: **2303.10798** (2023).
[27] T. Horiyama, Y. Okamoto, and R. Uehara, Ls in L and sphinxes in sphinx, IPSJ (International Processing Society of Japan) SIG Technical Report (Corrected in Horiyama's thesis) **2015-AL-154** (2015-09-28).
[28] Online Encylopedia of Integer Sequences A279887: Number of tilings of a sphinx of order n by elementary sphinxes, oeis.org/A279887 (2023).
[29] N. S. Izmailian, V. V. Papoyan, and R. M. Ziff, Exact finite-size corrections in the dimer model on a planar square lattice, J. Phys. A: Math. Th. **52**, 335001 (2019).
[30] I. Kanemoto and T. Saitoh, Improving the lower bounds of the number of tilings for Ls in L and sphinxes in sphinx: Enumerating tilings by frontier-based search, IPSJ (International Processing Society of Japan) SIG Technical Report **2016-AL-158** (2016-06-17).
[31] Online Encylopedia of Integer Sequences A070765: Number of polyiamonds with n cells, without holes, oeis.org/A070765 (2023).
[32] N. Metropolis, A. W. Rosenbluth, M. N. Rosenbluth, A. H. Teller, and E. Teller, Equation of state calculations by fast computing machines, J. Chem. Phys. **21**, 1087 (2004).
[33] L. Pauling, The structure and entropy of ice and of other crystals with some randomness of atomic arrangement, J. Am. Chem. Soc. **57**, 2680 (1935).
[34] H. N. V. Temperley and E. H. Lieb, Relations between the 'percolation' and 'colouring' problem and other graph-theoretical problems associated with regular planar lattices: Some exact results for the 'percolation' problem, Proc. Roy. Soc. London. Ser. A **322**, 251 (1971).
[35] D. L. Caspar and A. Klug, Physical principles in the construction of regular viruses, Cold Spring Harbor Symposia on Quantitative Biology **27**, 1 (2018).
[36] P. G. Stockley and R. Twarock, eds., in *Emerging Topics in Physical Virology* (Imperial College Press, London, 2010).

Supplemental Material: Riddles of the sphinx tilings

Greg Huber*
Chan Zuckerberg Biohub – San Francisco, 499 Illinois Street, San Francisco, CA 94158, USA

Craig Knecht†
691 Harris Lane, Gallatin, TN 37066, USA

Walter Trump‡
Department of Physics, Gymnasium Stein, Faber-Castell-Allee 10, 90547 Stein, Germany

Robert M. Ziff§
Center for the Study of Complex System and Department of Chemical Engineering, University of Michigan, Ann Arbor, MI 48109-2800, USA

(Dated: May 2, 2023)

Here we have figures illustrating various definitions and results for the sphinx tilings. The explanations and discussions are given in the captions of the figures. Figs. S1–S3 show various definitions and representations used in this work. Fig. S4 shows the tiling of an order-6 frame with charge (A vs. V) highlighted. Fig. S5 shows details of the seam method for the seam in Fig. 3 of the main text. Fig. S6 concerns the asymptotic behavior of the plot in Fig. 4. Fig. S7 shows the 36 sphinx orientations around a given triangle used in the heat map in Fig. 5. Figs. S8 and S9 show the frames and tilings of dyad, and Fig. S10 shows all 153 tilings of an order-5 sphinx frame. Figs. S11–S14 show higher-order polyads of orders 7–10. Figs. S15–S17 show some properties of tilings on an order-7 frame. Figs. S18 shows the energy and chirality of an order-7 sphinx and relates to Fig. 13. Figs. S19 shows a tiling of a 12-order frame by triangular sub-units, Fig. S20 concerns a 23-order frame, and the final figure, Fig. S21, shows a tiling of a 100-order frame generated by MC.

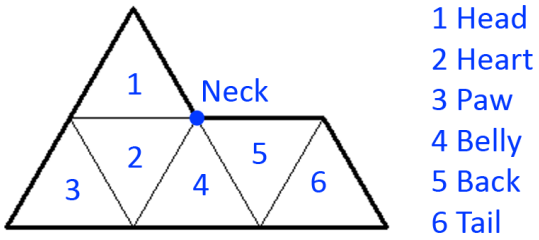

Fig. S1. The six faces of the sphinx hexiamond in its canonical state, and anatomical names that we assign to them.

* gerghuber@gmail.com
† craigknecht03@gmail.com
‡ w@trump.de
§ rziff@umich.edu

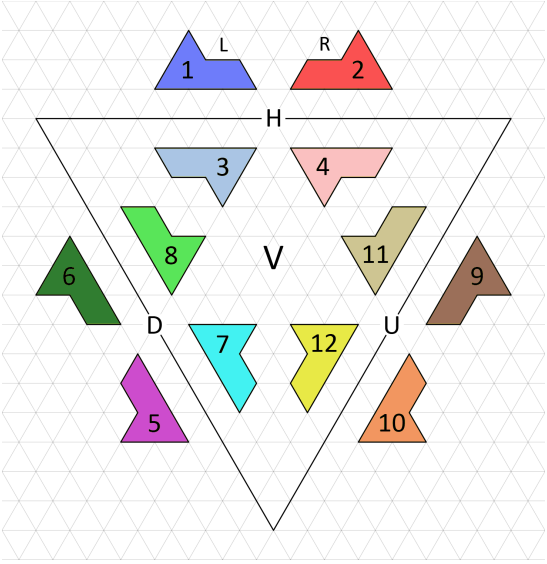

Fig. S2. Standard colors and numerical designations for the 12 different states of a sphinx tile.

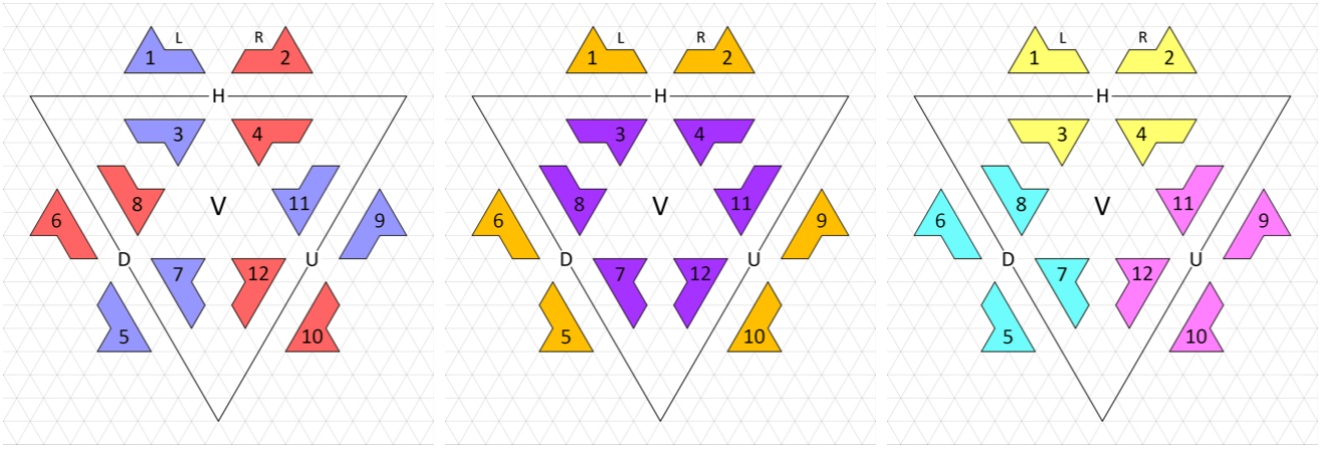

Fig. S3. Special colors used to distinguish certain tile properties. Left: Chirality, L = left (blue), R = right (red); Middle: Charge, A (+) (amber), V (−) (violet), see also Fig. S4; Right: Base slope, 0° (H) (yellow), +60° (U) (magenta), −60° (D) (turquoise).

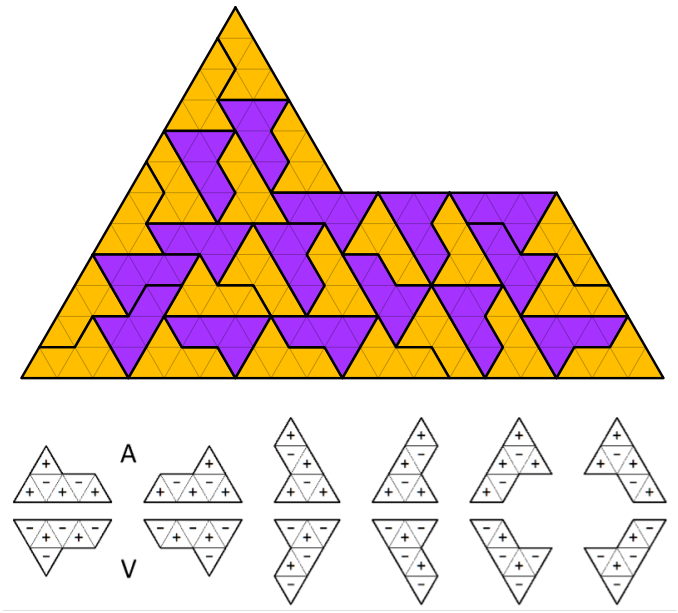

Fig. S4. Above: Tiling of a sixth-order sphinx, with A-sphinxes (colored in amber) and V-sphinxes (colored in violet). Below: Illustrations of the A- and V-tile orientations, where + and − represent A- and V-triangles respectively.

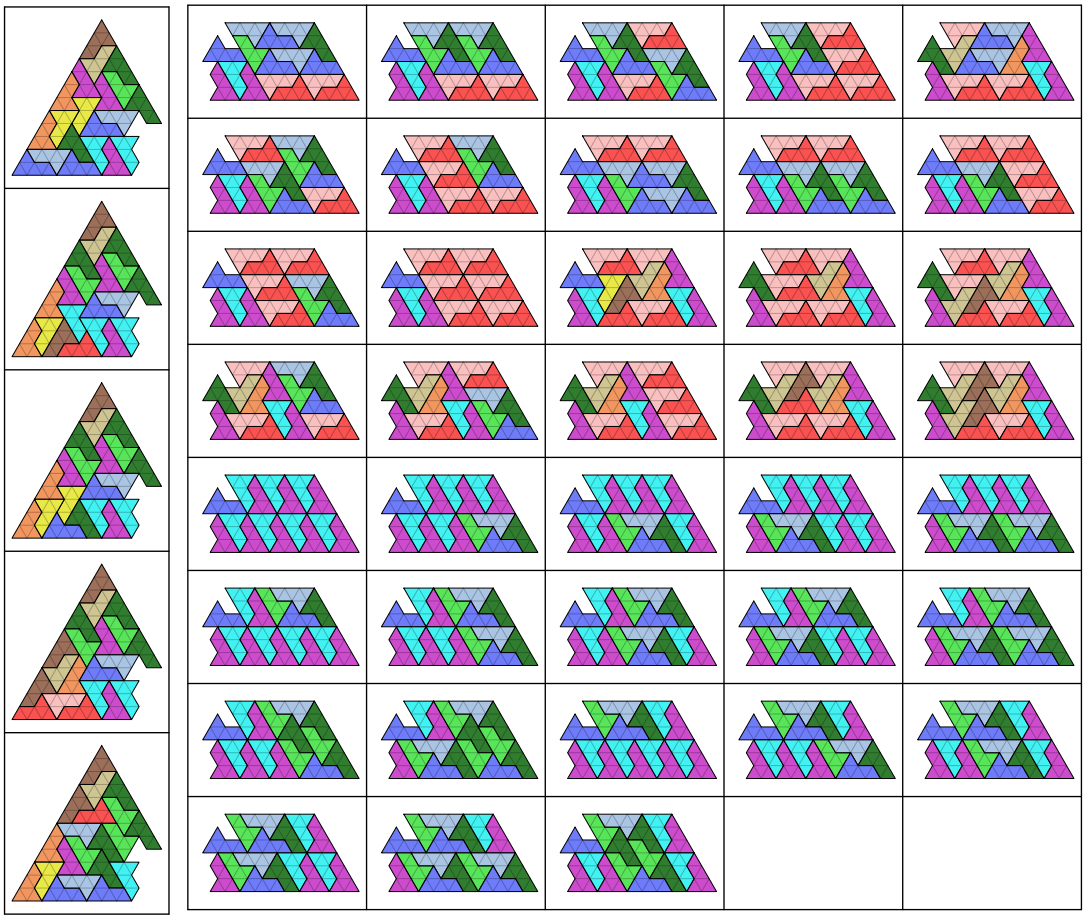

Fig. S5. Seam method for a sphinx of order 6. For this seam, shown in Fig. 3 in the main text, there are 5 tilings for the left part and 38 tilings for the right part as shown above, yielding a total of $5 \cdot 38 = 190$ tilings. For this order sphinx, there are a total of 145 possible seams and a total of 71,838 tilings.

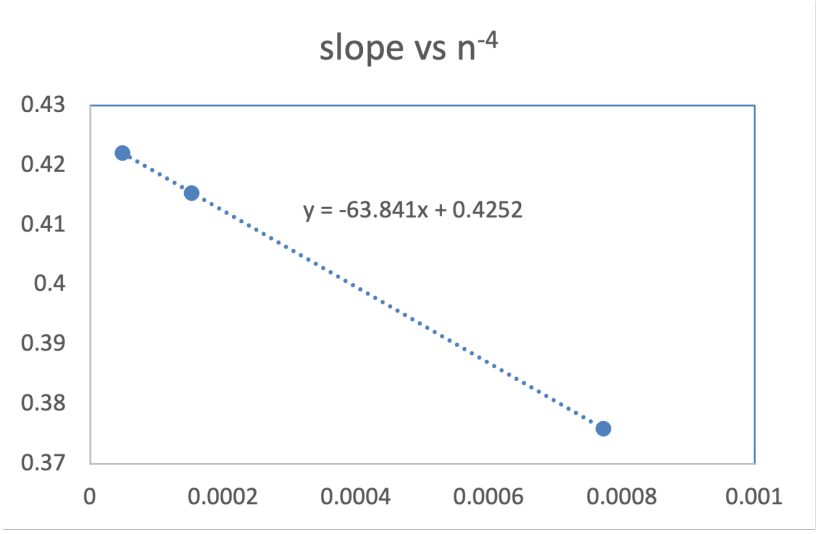

Fig. S6. A plot of the slopes in Fig. 4 in the main text vs. $1/n^4$. The equations of the linear fits in Fig. 4 are: $\ln N = 0.2288n^2 - 0.7508$ (n = 3–5), $\ln N = 0.3759n^2 - 2.5114$ (n = 6–8), $\ln N = 0.4154n^2 - 3.703$ (n = 9–11), and $\ln N = 0.4221n^2 - 2.0353$ (n = 12,13). This figure shows a plot of the three latter slopes as a function of $1/n^4 = 1/\text{area}^2$, implying $N \sim \exp(0.425n^2 - 63.8/n^2) \sim \sigma^{n^2}$ for large N, where $\sigma = 1.53(1)$ is the "sphinx constant." For comparison, in the case of the Aztec diamond, the number of domino tilings is exactly given by $N = (\sqrt{2})^A$, where $A = n(n+1)$ is the area of the Aztec diamond in domino units, expressed in terms of the order n of the diamond (see Refs. [10,11] in the main text).

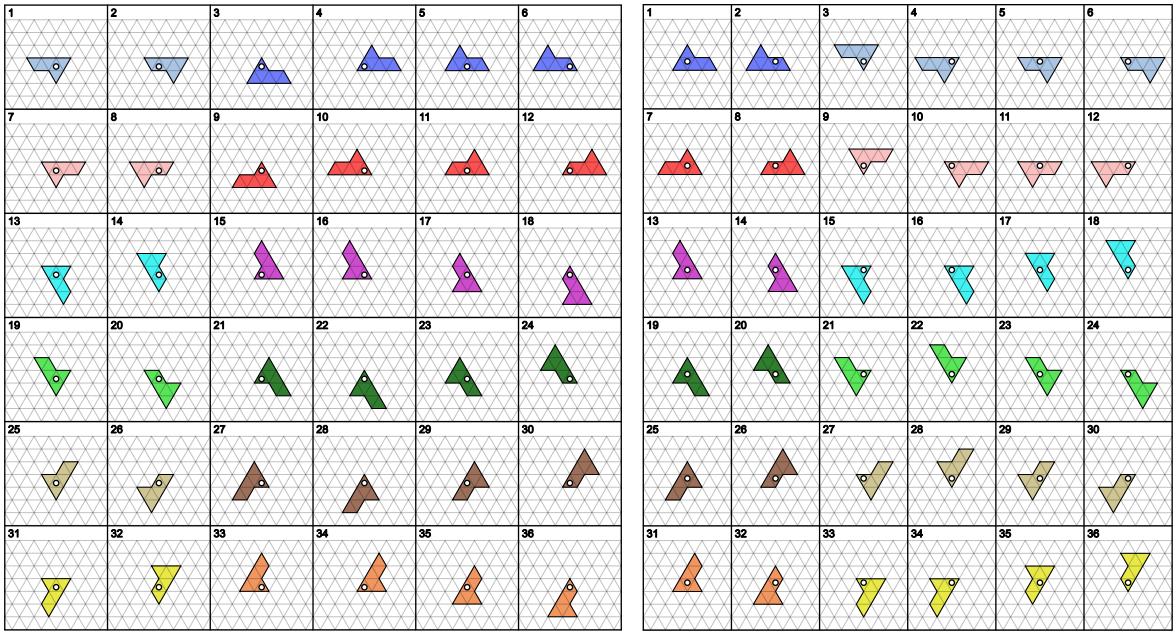

Fig. S7. Each 'A' (△) and 'V' (▽) grid triangle and can be covered in 36 ways by a sphinx tile. Depending on its orientation, a sphinx tile has 2 (or 4) A-faces and 4 (or 2) V-faces. A given A- or V-triangle may be covered by one of the 6 faces of a sphinx tile in one of 12 states. In the graphics above, the given triangle is marked by a circle, with a central A-triangle on the left and a central V-triangle on the right. The prevalence of these tiles in tilings of S7 is shown in Fig. 5 in the main text.

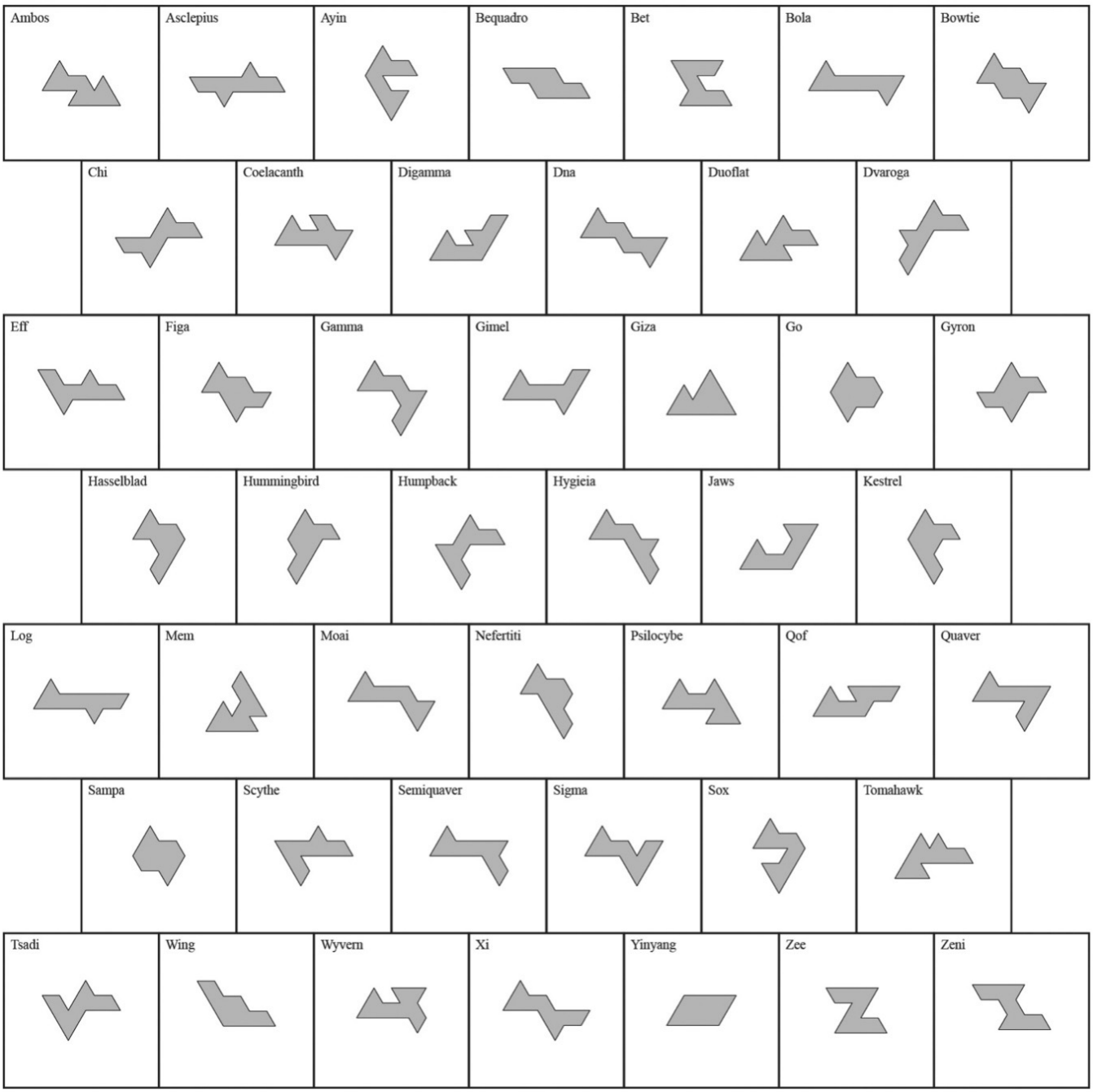

Fig. S8. The 46 different free sphinx dyads, which are size-2 polyiamonds with area 12 (in units of triangular area), which can be tiled by two sphinx tiles. "Free" means distinct up to rotation and reflection. They have been arranged alphabetically by the names we have given them.

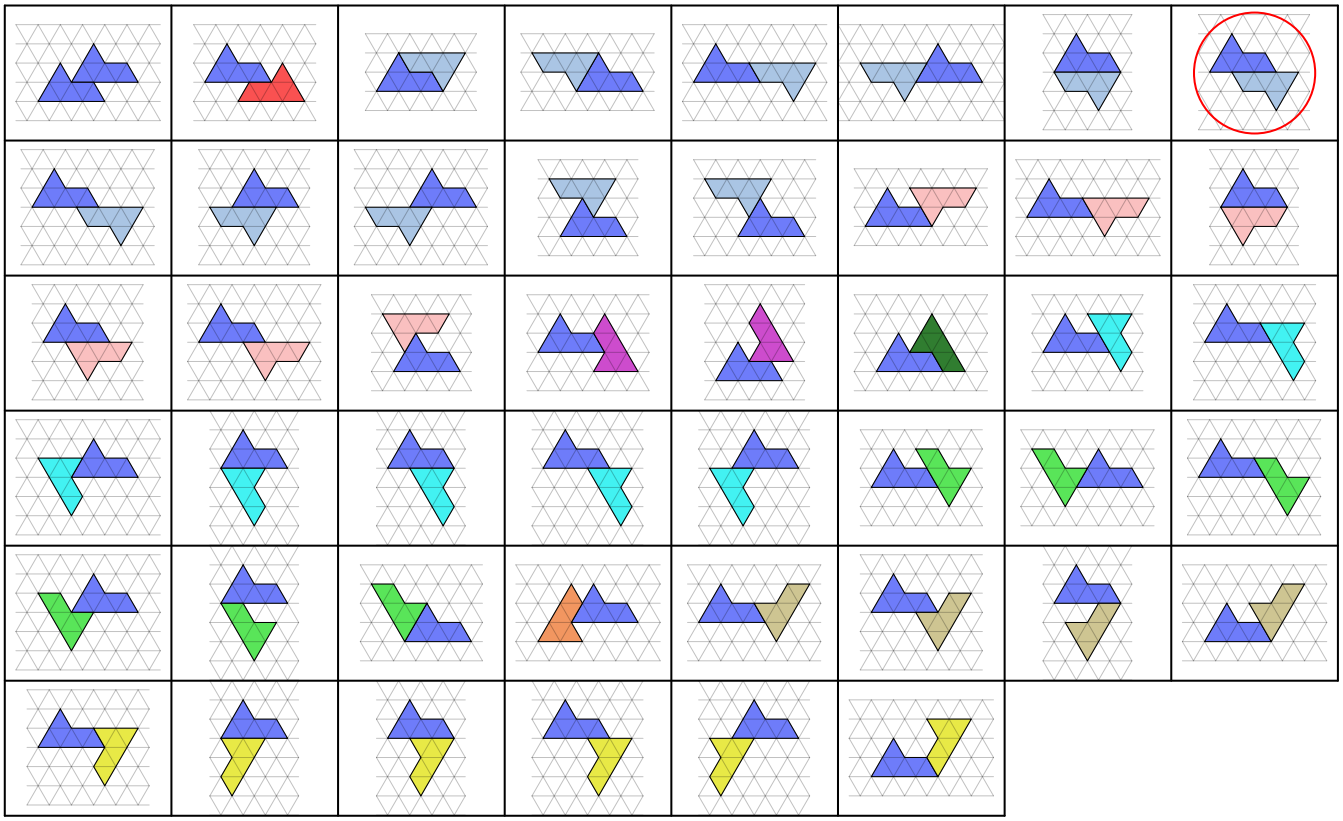

Fig. S9. The free tilings of the 46 sphinx dyads of Fig. S8. The dark blue sphinx tile is in the canonical state. Here the dyads are sorted by the state of the second tile, which is shown in the color spectrum of Fig S2. The bowtie (in the red circle) is the only dyad with two different fixed tilings; the second tiling is a mirror reflection of the one shown here.

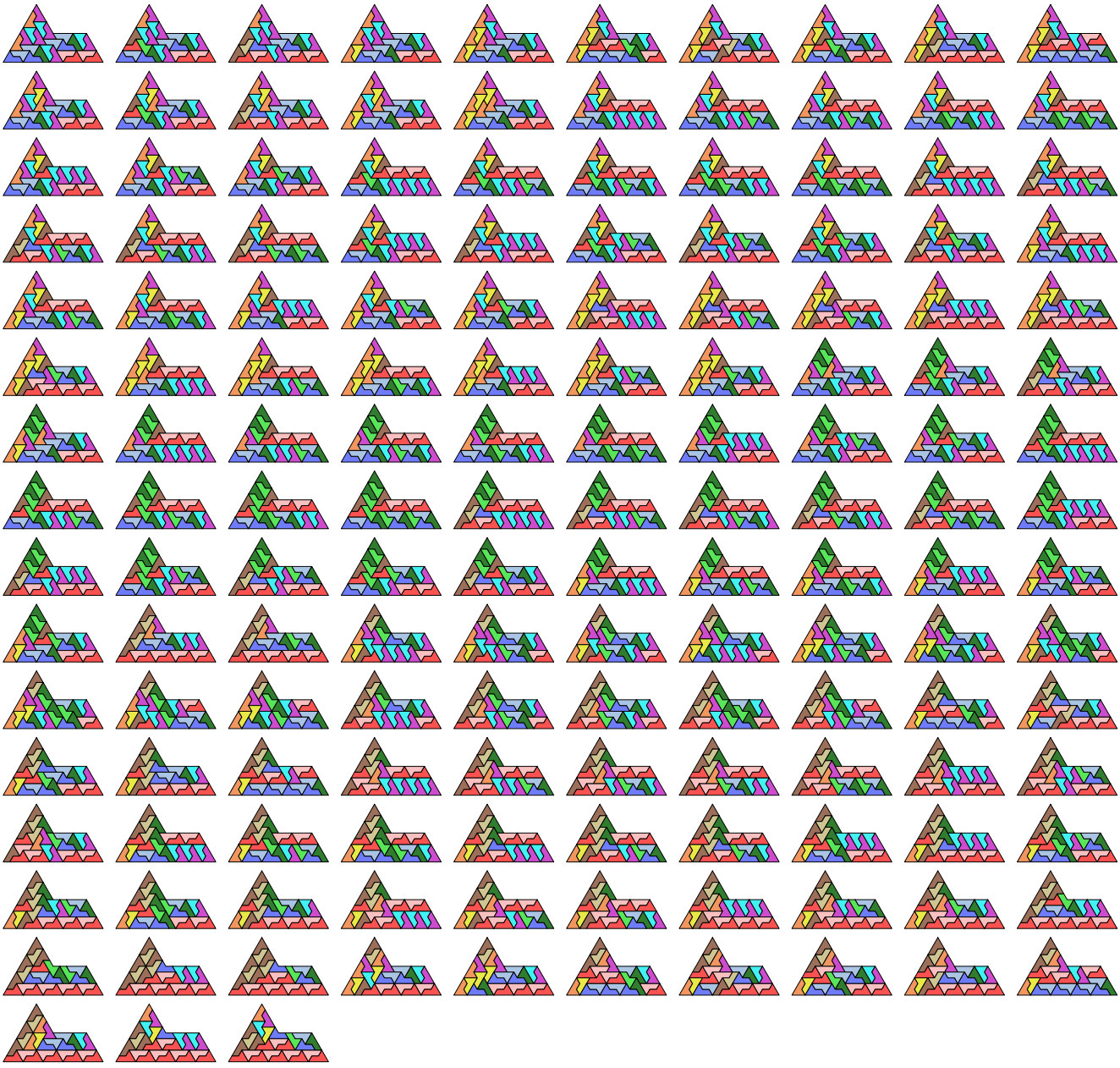

Fig. S10. The 153 sphinx tilings of an order-5 sphinx frame in the canonical state, using the colors of Fig. S2.

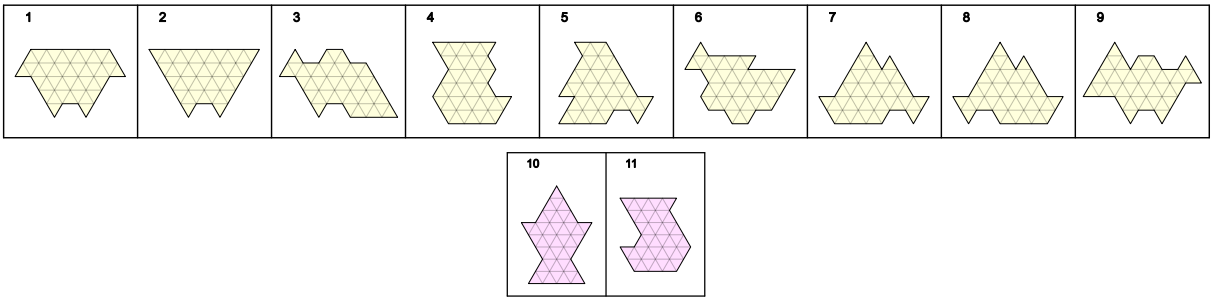

Fig. S11. Fundamental heptads (polyads of size 7). Heptads found in tilings of order-7 sphinx frames (yellow color above), and two additional heptads not found in the order-7 tilings (but in tilings of a sphinx of order 8) (purple color below).

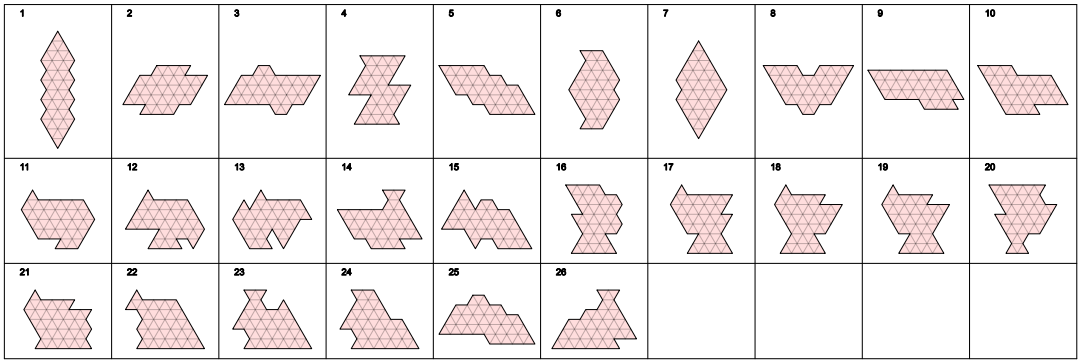

Fig. S12. Fundamental octads (polyads of size 8) found in order-7 sphinx tilings.

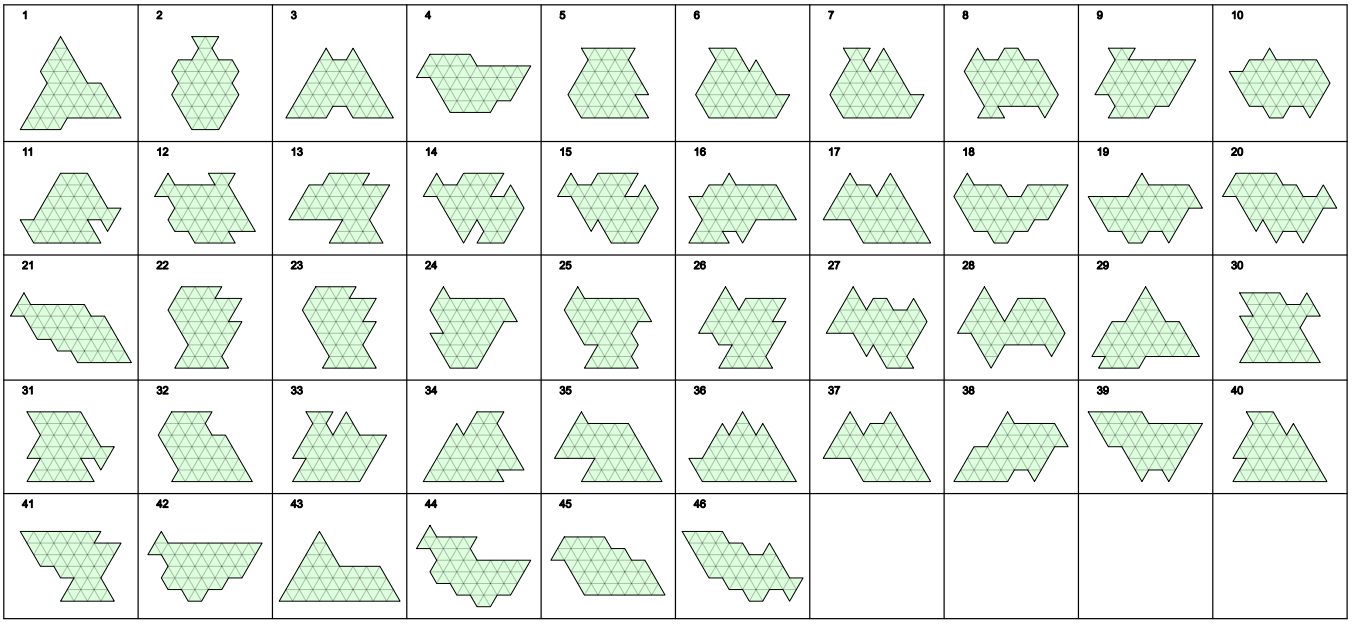

Fig. S13. Fundamental enneads (polyads of size 9) found in order-7 sphinx tilings. Number 1 is the "mystical triode" (Fig. 9). Number 43 is the sphinx frame of order 3 shown in Fig. 2, where the bottom right tiling in that figure has no common tiles with the other three tilings of the S3 frame, making this polyad fundamental.

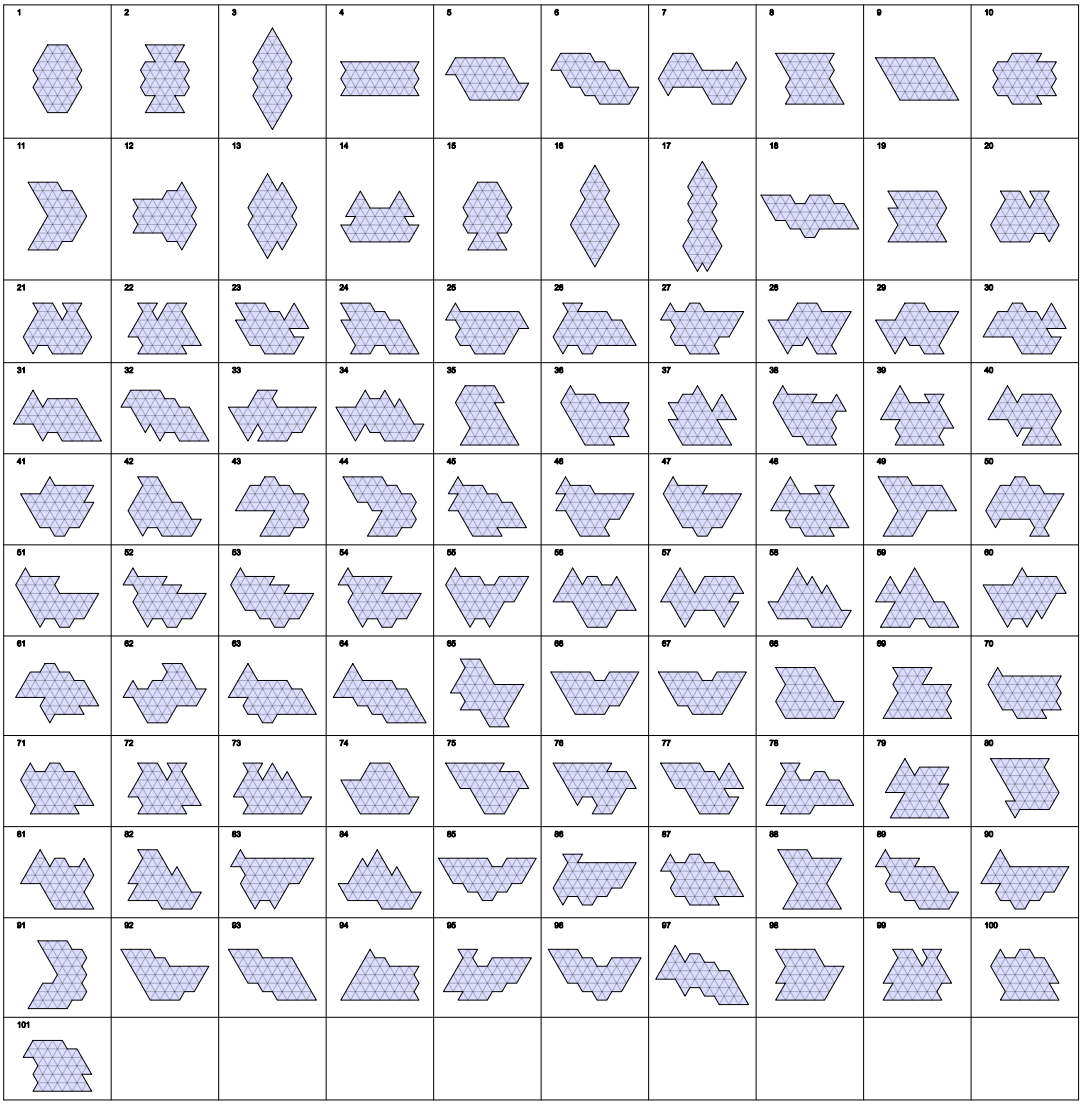

Fig. S14. Fundamental decads (polyads of size 10) found in order-7 sphinx tilings.

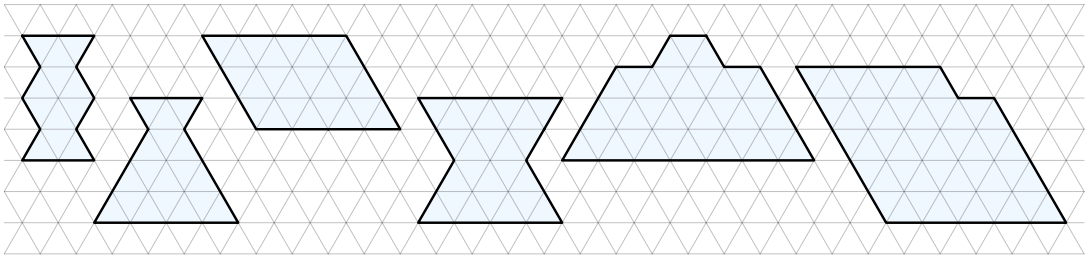

Fig. S15. Except for the two tilings in Fig. S16, all 5 965 398 sphinx tilings of an order-7 sphinx frame contain at least one of these 6 fundamental polyads (of orders 2, 3, 4, 4, 6 and 8 respectively). Furthermore, there are only seven tilings of the order-7 sphinx lacking the first 5 polyads above.

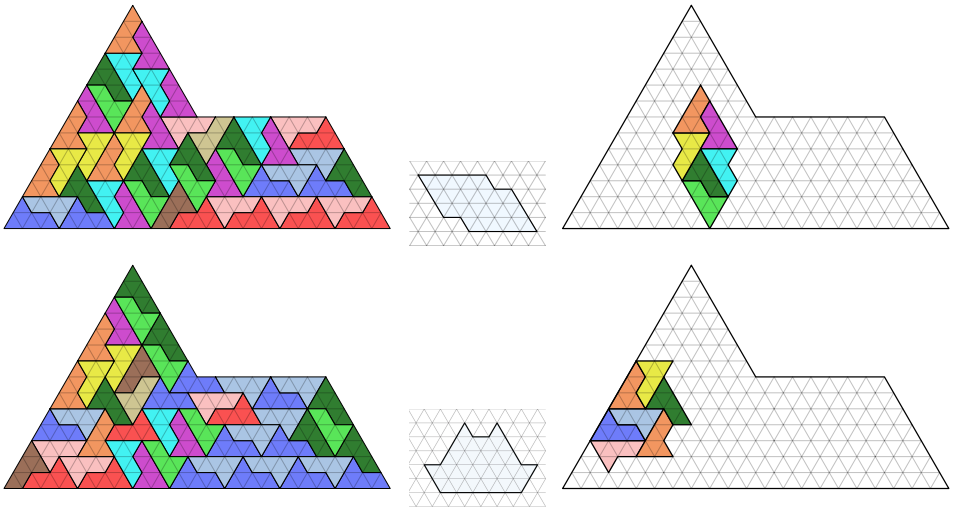

Fig. S16. The only two tilings of an S7 frame that do not contain any of the six fundamental polyads of Fig. S15. Here, the tilings contain a fundamental hexad (upper figure) and heptad (lower figure) as shown to the right of each tiling.

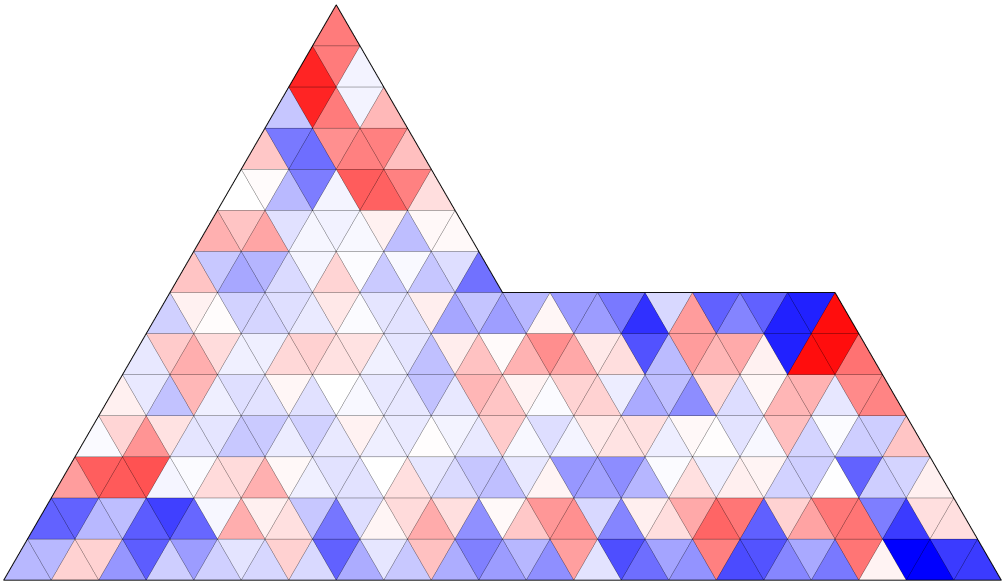

Fig. S17. Chirality distribution in all 5 965 398 tilings of an order-7 sphinx frame by sphinx tiles. Darker blue means that the grid triangle is statistically covered by more sphinx tiles with left chirality than with right chirality. Triangles with red color are covered by more right than left chiral tiles. White triangles represent equal coverage by left and right chiral tiles.

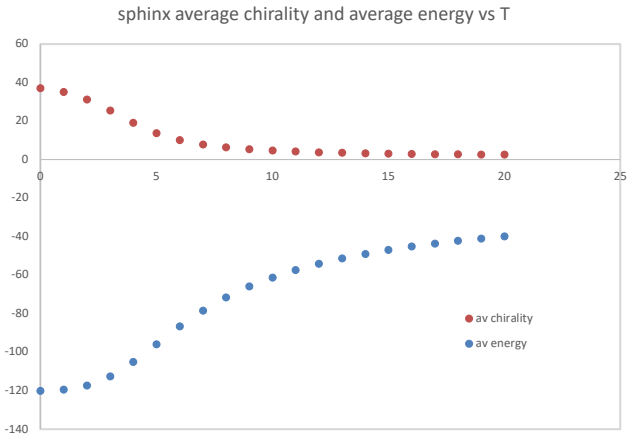

Fig. S18. The average energy and average chirality as a function of temperature, calculated from the exact enumeration of all 5 965 398 tilings of an order-7 sphinx (S7). To find these quantities, we used $\langle E\rangle = \sum_E n(E)Ee^{-E/T}/Q(T)$ and $\langle\chi\rangle = \sum_E n(E)\chi(E)\,e^{-E/T}/Q(T)$ where $\chi(E)$ is the average chirality (L−R) of samples of energy E, $Q(T) = \sum_E n(E)e^{-E/T}$, and where we took $J = 1$ and $k_B = 1$ for a dimensionless temperature T. Notice that for S7, the chirality is always positive and increases as the temperature is decreased, while for S23 we find a negative chirality in our MC simulations.

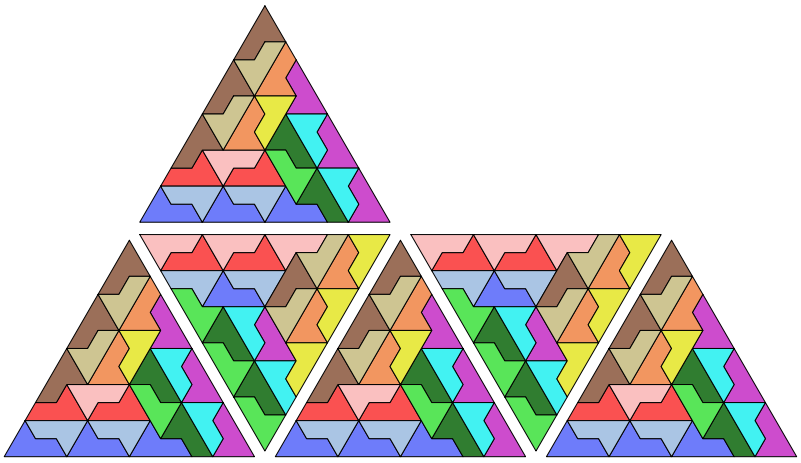

Fig. S19. Twelve is the smallest order of a sphinx frame where a tiling exists in which each of the six order-12 triangles (T12) is tiled by sphinx tiles. Equilateral triangles smaller than order 12 cannot be tiled by sphinxes. This method of substitution, using all 830 tilings of T12, generates 830^6 distinct sphinx tilings. Although this represents over 3.2×10^{17} tilings, it still accounts for only about one hundred millionth of all order-12 sphinx tilings.

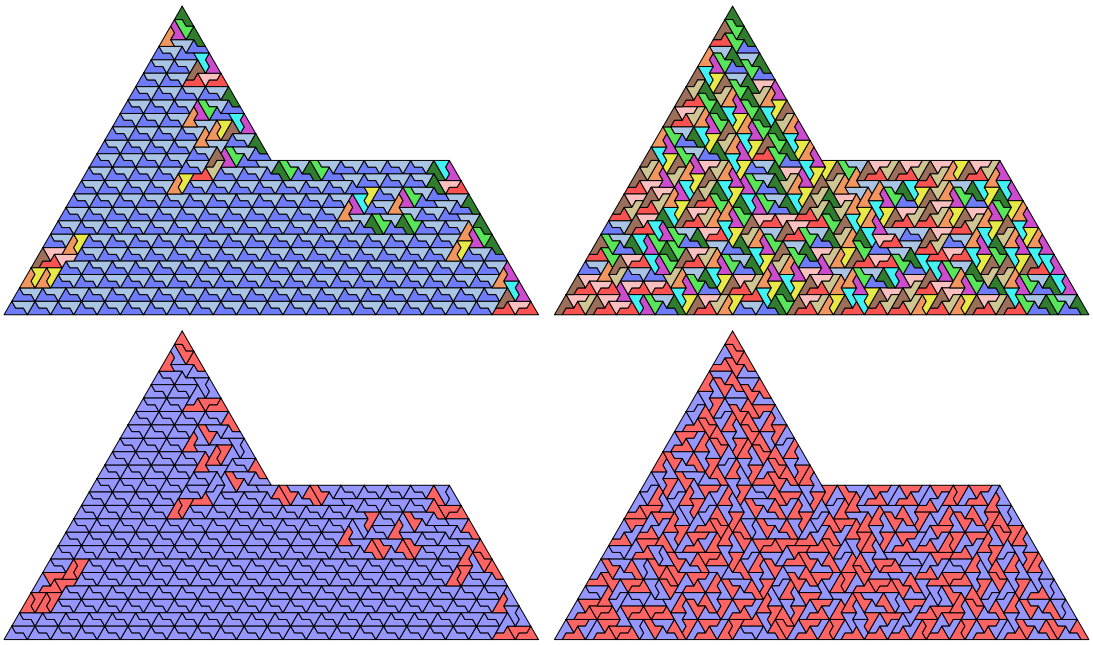

Fig. S20. Tiling realizations of an order-23 sphinx frame for low and high chiral energy, found with the Monte Carlo method. Top left: low energy, top right: high energy. Bottom row: the same tilings as the top row, but with L tiles shown in blue and R tiles shown in red.

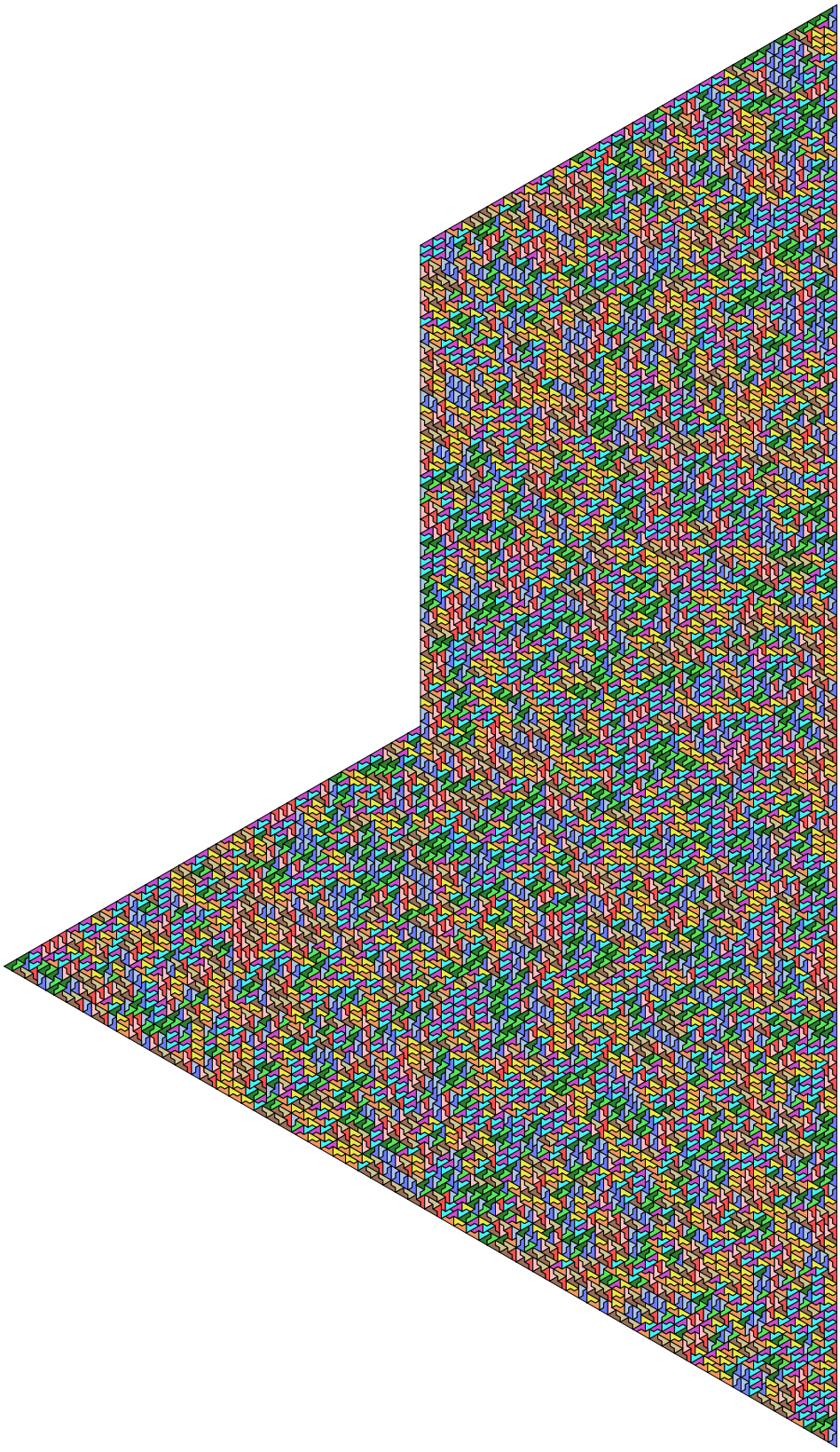

Fig. S21. A typical tiling of an order-100 sphinx frame generated by the fundamental polyad MC algorithm.